Numerical Heat Transfer, Part B, 43: 19–41, 2003

1040-7790/03 $12.00 + .00
DOI: 10.1080/10407790390122005

Taylor & Francis
Taylor & Francis Group

# A NEW HIGH-ORDER-ACCURATE AND BOUNDED SCHEME FOR INCOMPRESSIBLE FLOW

***Jin-Jia Wei, Bo Yu, and Wen-Quan Tao***
*School of Energy & Power Engineering, Xi'an Jiaotong University, Xi'an, People's Republic of China*

***Yasuo Kawaguchi***
*Turbomachinery Research Group, Institute for Energy Utilization, National Institute of Advanced Industrial Science and Technology, Ibaraki, Japan*

***Huang-sheng Wang***
*Department of Engineering, Queen Mary, University of London, London, United Kingdom*

***The interpolative reasonableness is analyzed and the conditions for the construction of bounded, accurate scheme with interpolative reasonableness (BAIR) are presented. It is required that the interfacial variable have a positive response to the disturbance occurring at the main grid point and that the transportive property be kept (dynamic interpolate reasonableness, DIR). A new high-order-accurate and bounded (HOAB) scheme based on the BAIR is proposed for the calculation of incompressible flow. The new scheme, HOAB, is tested by five problems: (1) pure convection of a stepwise profile in an oblique uniform velocity field, (2) pure convection of a double-step profile in an oblique uniform velocity field, (3) pure convection of an elliptical profile, (4) lid-driven cavity flow, and (5) turbulent flow over a backward-facing step. The computational results are compared with the results of five high-resolution schemes: Zhu and Rodi's MINMOD scheme, Van leer's CLAM scheme, Chakravarthy and Osher's OSHER scheme, Gaskell and Lau's SMART scheme, Darwish's STOIC scheme, and exact solution/benchmark solution or experimental data. The numerical tests show that the new scheme is capable of capturing steep gradients while maintaining boundedness of solutions and is more accurate than the other five high-resolution schemes.***

## INTRODUCTION

Upwind-based lower-order schemes such as the power-law scheme were popular because they are absolutely stable and possess boundedness. Physically plausible

Received 11 April 2002; accepted 7 June 2002.

This work is supported by the National Key Project of Fundamental R&D of China (Grant 2000026303) and the National Natural Science Foundation of China (Grant 50076034).

Address correspondence to W.-Q. Tao, School of Energy & Power Engineering, Xi'an Jiaotong University, Xi'an 710049, People's Republic of China. E-mail: wqtao@xjtu.edu.cn

## NOMENCLATURE

| | | | |
|---|---|---|---|
| $A$ | coefficients in the discretized equation | $\varepsilon$ | dissipation of turbulent kinetic energy |
| $b$ | source term | $\mu$ | dynamic viscosity |
| $C_{IF}$ | convective influx | $\rho$ | density |
| $f$ | relationship function | $\phi$ | general dependent variable |
| $H$ | step height in problem 5 | | |
| $k$ | turbulent kinetic energy | **Subscripts** | |
| $L$ | characteristic length of cavity | $C$ | central grid point |
| | | $D$ | downstream grid point |
| $S$ | source term | $e$, $w$ | cell faces |
| Re | Reynolds number | $EE$, $E$, $W$, $P$, $N$, $S$ | main grid points |
| $u$, $v$ | velocity component in $x$ and $y$ coordinates | $f$ | cell faces |
| | | NB | neighbor grid point |
| $x$, $y$ | spatial coordinates | $R$ | reattachment |
| $\alpha$ | variable parameter in Eq. (3) | $U$ | upstream grid point |
| $\Gamma$ | generalized diffusion coefficient | **Superscript** | |
| $\Delta x$ | cell dimension | $\hat{}$ | a normalized variable |

numerical results can be predicted by using them for strong convection computations. Recently, however, the lower-order schemes have received ever-increasing criticism because of their well-known deficiency of being highly diffusive [1–3]. On the other hand, high-order schemes such as the central difference scheme and the QUICK scheme can provide higher-accuracy numerical solutions. Here by high-order schemes we mean schemes which possess at least second-order accuracy of the truncation error. They have been used more and more widely nowadays. However, they often suffer from the drawbacks of oscillatory or overshoot/undershoot behavior when grid Peclet number is larger than some limit or there exists a sharp change of profile in the computational domain. In order to overcome these shortcomings of high-order schemes, many efforts have been made which led to the development of high-resolution (HR) schemes. High-resolution schemes based on convective boundedness criteria (CBC) proposed by Gaskell and Lau [4] can provide numerical solution with high accuracy while removing overshoot/undershoot or nonphysical oscillatory behavior. Therefore, how to construct a high-order-accurate and bounded scheme becomes significant in the field of numerical heat transfer/computational fluid dynamics (NHT/CFD). Many high-resolution schemes have been proposed, such as MINMOD [5], CLAM [6], OSHER [7], SMART [4], STOIC [8], and WACEB [9]. Especially the STOIC scheme was found to be the most accurate high-order scheme without undue physical oscillations or numerical smearing.

Since Gaskell and Lau's CBC can only guarantee the boundedness, without any constraint to the accuracy, it is useful to consider further how to construct the definition line(s) (hereafter, characteristic line for simplicity) in the normalized variable diagram (NVD) such that the resulting scheme has both boundedness and high accuracy.

The objective of this study is (1) to find the conditions for the construction of a bounded, accurate scheme from the viewpoint of interpolation reasonableness

(BAIR), (2) to propose a new high-order-accurate and bounded (HOAB) scheme based on BAIR and compare the HOAB scheme with other high-resolution schemes for both pure convection and laminar and turbulent convection-diffusion problems.

## HIGH-ORDER SCHEMES IN NUMERICAL DISCRETIZATION OF THE TRANSPORT EQUATION

For simplicity, a one-dimensional incompressible governing equation is adopted to show numerical discretization of the transport equation. The extension to two or three dimensions is simple and straightforward. A finite-volume method is used to discretize the following transport equation on a uniform grid system as shown in Figure 1:

$$\frac{\partial \rho u \phi}{\partial x} = \frac{\partial}{\partial x}\left(\Gamma \frac{\partial \phi}{\partial x}\right) + S \tag{1}$$

where $u$ is the velocity, $\phi$ is any dependent variable, and $\rho$ , $\Gamma$, and $S$ are the density, diffusion coefficient, and source term, respectively.

Integrating Eq. (1) over a control volume as shown in Figure 1, we have

$$\frac{(\rho u)_e \phi_e - (\rho u)_w \phi_w}{\Delta x} = \frac{\Gamma_e[(\phi_E - \phi_P)/\Delta x] - \Gamma_w[(\phi_P - \phi_W)/\Delta x]}{\Delta x} + S_p \tag{2}$$

In the above equation, the diffusive term is discretized by a second-order central difference scheme. As for the convective term, some well-known high-order schemes have been proposed to get higher accurate solution, such as the second-order upwind difference scheme (SUD), the central difference scheme (CD), the Fromm scheme [10], the QUICK scheme [11], and the third-order upwind difference scheme (TUD). For the QUICK scheme,

$$\begin{aligned} &\text{For } u_e \geq 0, \quad \phi_e^+ = -0.125\phi_W + 0.75\phi_P + 0.375\phi_E \\ &\text{For } u_e < 0, \quad \phi_e^- = -0.125\phi_{EE} + 0.75\phi_E + 0.375\phi_P \end{aligned} \tag{3}$$

It is well known that the QUICK scheme is a third-order-accurate approximation, $O(\Delta x^3)$, for the cell-face interpolation. By introducing a second-order curvature compensation,

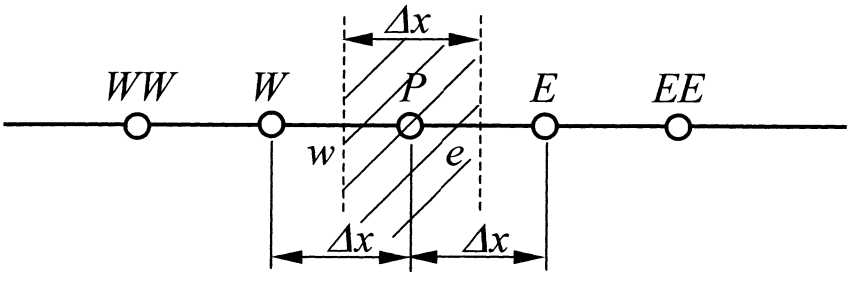


**Figure 1.** Uniform grid system.

$$\begin{aligned} &\text{For } u_e \geq 0, \quad \text{Curv}^+ = \alpha_e^+(\phi_w - 2\phi_p + \phi_E) \\ &\text{For } u_e < 0, \quad \text{Curv}^- = \alpha_e^-(\phi_{EE} - 2\phi_E + \phi_P) \end{aligned} \tag{4}$$

to the third-order-accurate approximation of $\phi_e$ in Eq. (3), a general form for all the high-order schemes can be expressed as [4]

$$\begin{aligned} &\text{For } u_e \geq 0, \quad \phi_e^+ = -(0.125 + \alpha_e^+)\phi_W + (0.75 + 2\alpha_e^+)\phi_P + (0.375 - \alpha_e^+)\phi_E \\ &\text{For } u_e < 0, \quad \phi_e^- = -(0.125 + \alpha_e^-)\phi_{EE} + (0.75 + 2\alpha_e^-)\phi_E + (0.375 - \alpha_e^-)\phi_P \end{aligned} \tag{5}$$

where $\alpha_e$ is a finite-variable parameter and the leading truncation error in Eq. (3) is $O(\alpha_e \Delta x^2)$. Table 1 lists $\alpha_e$ values for several well-known high-order schemes. The accuracy increases with decrease of the absolute value of $\alpha_e$, and $\alpha_e = 0$ is indicative of the maximum accuracy obtainable, $O(\Delta x^3)$.

Similarly, we have

$$\begin{aligned} &\text{For } u_w \geq 0, \quad \phi_w^+ = -(0.125 + \alpha_w^+)\phi_{WW} + (0.75 + 2\alpha_w^+)\phi_W + (0.375 - \alpha_w^+)\phi_P \\ &\text{For } u_w < 0, \quad \phi_w^- = -(0.125 + \alpha_w^-)\phi_E + (0.75 + 2\alpha_w^-)\phi_P + (0.375 - \alpha_w^-)\phi_W \end{aligned} \tag{6}$$

where $\alpha_w$ is the corresponding value of the variable $\alpha$ at the left-hand face of the control volume centered at node P.

All these convection schemes can be written in a general compact form as follows:

$$\begin{aligned} &\text{For } u_e \geq 0, \quad \phi_e^+ = \phi_P + (\phi_e^+ - \phi_P) \\ &\text{For } u_e < 0, \quad \phi_e^- = \phi_E + (\phi_e^- - \phi_E) \end{aligned} \tag{7}$$

Similarly, we have

$$\begin{aligned} &\text{For } u_w \geq 0, \quad \phi_w^+ = \phi_W + (\phi_w^+ - \phi_W) \\ &\text{For } u_w < 0, \quad \phi_w^- = \phi_P + (\phi_w^- - \phi_P) \end{aligned} \tag{8}$$

On the right-hand side of Eqs. (7) and (8), the first term is the first-order upwind difference scheme (FUD) and the second term is the difference between the adopted scheme and the first-order upwind scheme. The first term is used to form the discretized equation coefficients and the second term is evaluated in the source term. This approach was first reported by Khosla and Rubin [12] and is called as deferred-correction technique. By using this technique, the resulting discretized equation is diagonally dominant.

Substituting Eqs. (7) and (8) into Eq. (2) and rearranging the equation, we have

$$\begin{aligned} &\left\{\frac{\Gamma_e}{\Delta x} + \frac{\Gamma_w}{\Delta x} + \max[(\rho u)_e, 0] + \max[-(\rho u)_w, 0]\right\}\phi_P \\ &\quad = \left\{\frac{\Gamma_e}{\Delta x} + \max[-(\rho u)_e, 0]\right\}\phi_E + \left\{\frac{\Gamma_w}{\Delta x} + \max[(\rho u)_w, 0]\right\}\phi_W + S_p \Delta x \\ &\qquad - \max[(\rho u)_e, 0](\phi_e^+ - \phi_P) + \max[-(\rho u)_e, 0](\phi_e^- - \phi_E) \\ &\qquad + \max[(\rho u)_w, 0](\phi_w^+ - \phi_W) - \max[-(\rho u)_w, 0](\phi_w^- - \phi_P) \end{aligned} \tag{9}$$

**Table 1.** Values of $\alpha$ for various well-known high-order schemes

| Scheme | CD | SUD | QUICIK | Fromm | TUD |
|---|---|---|---|---|---|
| $\alpha$ | $-0.125$ | 0.375 | 0 | 0.125 | 1/24 |

Considering mass conservation,

$$\max[(\rho u)_e, 0] + \max[-(\rho u)_w, 0] = \max[-(\rho u)_e, 0] + \max[(\rho u)_w, 0] \tag{10}$$

we obtain the final discretized equation as follows:

$$A_P \phi_P = A_E \phi_E + A_W \phi_W + b \tag{11}$$

$$A_E = \frac{\Gamma_e}{\Delta x} + \max[-(\rho u)_e, 0], \quad A_W = \frac{\Gamma_w}{\Delta x} + \max[(\rho u)_w, 0], \quad A_P = A_E + A_W$$

$$b = S_p \Delta x + \left\{ \begin{array}{l} -\max[(\rho u)_e, 0](\phi_e^+ - \phi_P) + \max[-(\rho u)_e, 0](\phi_e^- - \phi_E) \\ +\max[(\rho u)_w, 0](\phi_w^+ - \phi_W) - \max[-(\rho u)_w, 0](\phi_w^- - \phi_P) \end{array} \right\}$$

It is noted that the second term in $b$ results from the adoption of the deferred-correction procedure.

## CONVECTIVE BOUNDEDNESS CRITERIA (CBC)

The symbols $U$, $C$, $D$, and $f$ in Figure 2 refer to the upstream, central, downstream node, and cell face, respectively. Any convective scheme using the values at the three nodes ($U$, $C$, and $D$) to interpolate the cell face value can be written in the following general form:

$$\phi_f = f(\phi_U, \phi_C, \phi_D) \tag{12}$$

Introducing the normalized variable [13]

$$\hat{\phi} = \frac{\phi - \phi_U}{\phi_D - \phi_U} \tag{13}$$

Eq. (13) becomes

$$\hat{\phi}_f = f(\hat{\phi}_U, \hat{\phi}_C, \hat{\phi}_D) \tag{14}$$

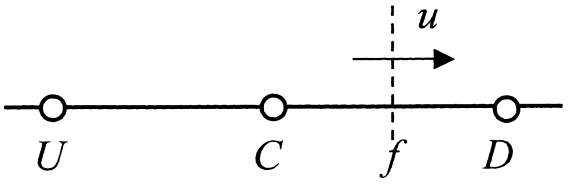


**Figure 2.** Interface and its related grid points for defining a normalized variable.

Noticing that $\hat{\phi}_U = 0, \hat{\phi}_D = 1$, Eq. (14) is simplified as

$$\hat{\phi}_f = f(\hat{\phi}_C) \tag{15}$$

Gaskell and Lau [4] proposed the convective boundedness criteria (CBC), which can be expressed as

(i) $f(\hat{\phi}_C)$ is a continuous function or union of piecewise continuous functions, and

$$\frac{df(\hat{\phi}_c)}{d\hat{\phi}_c} \geq 0 \tag{16}$$

(ii)

$$\begin{aligned} &f(\hat{\phi}_C) = 0 && \hat{\phi}_C = 0 \\ &f(\hat{\phi}_C) = 1 && \hat{\phi}_C = 1 \\ &\hat{\phi}_C \leq f(\hat{\phi}_C) \leq 1 && 0 < \hat{\phi}_C < 1 \\ &f(\hat{\phi}_C) = \hat{\phi}_C && \hat{\phi}_C < 0, \quad \hat{\phi}_C > 1 \end{aligned} \tag{17}$$

The above conditions can be clearly represented in the NVD as shown in Figure 3*a*. In this plot, the shaded area and the oblique line passing through points $(0, 0)$ and $(1, 1)$ are the regions that satisfy the criteria.

The CBC has long been accepted as both sufficient and necessary condition for a scheme possessing boundedness [4, 8]. Very recently, Yu et al. indicated that this is not the case [14], and they provided another CBC region in the NVD as shown in Figure 3*b*. By carefully examination of the two CBC regions, it can be seen that within $\tilde{\phi} \in [0., 1.0]$, the shaded area of Figure 3*a* is the sufficient and necessary

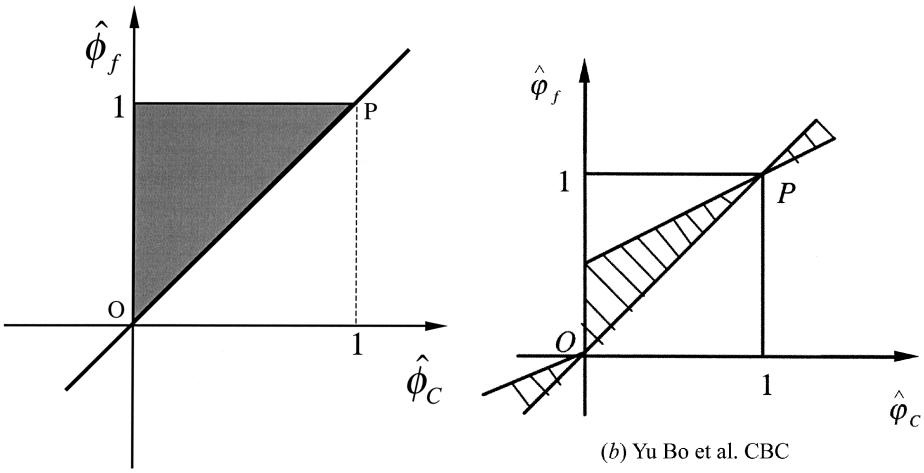


(*a*) Gaskell/Lau CBC

(*b*) Yu Bo et al. CBC

**Figure 3.** The region of convective boundedness criteria.

condition, while for $\tilde{\phi} < 0$ or $\tilde{\phi} > 1$ the Gaskell/Lau CBC is only sufficient, not necessary. This means that the definition lines in the region of $\tilde{\phi} < 0$ or $\tilde{\phi} > 1$ may not coincide with the diagonal. Our numerical results show that the solution accuracy of a scheme depends mainly on the definition line within $\tilde{\phi} \in [0., 1.0]$, therefore in following discussion we will take the diagonal as part of the definition lines outside $\tilde{\phi} \in [0., 1.0]$. Within $\tilde{\phi} \in [0., 1.0]$, how to construct the scheme definition lines is of great importance for the solution accuracy. Leonard [15] once demonstrated that if the definition line of a scheme goes through the point $Q$ $(0.5, 0.75)$ in the NVD, this scheme must have at least second-order accuracy. This gives a hint to construct a high-order scheme. However, more consideration is needed in order to delineate a region in the NVD within the range $\tilde{\phi} \in [0., 1.0]$ such that any scheme with its characteristic line within the newly delineated region is bounded and at least of second-order-accuracy.

## CONVECTIVE STABILITY

Stability of the discretized convective scheme is another important feature for the computation of incompressible flow. It can be shown that the CBC can guarantee the stability of a scheme. Actually, as shown in [16], the intersection between the characteristic line and the ordinate of the NVD is the reciprocal of the critical Peclet number of the scheme. Since the CBC requires that the characteristic line of a bounded scheme should go through the original point of the NVD, the satisfaction of the stability condition is embodied in the CBC, and will not be discussed separately.

In the following, focus will be put on the interpolative reasonableness from the viewpoint of an iterative solution procedure.

## INTERPOLATIVE REASONABLENESS

For a bounded interpolation in the normalized variable diagram, $\tilde{\phi}_f$ should be between $\tilde{\phi}_C$ and 1. This criterion gives the interpolative reasonableness with respect to static interpolation characteristics and is necessary for computed boundedness. The bounded interpolation is called static interpolative reasonableness (SIR) here. As is well known, the numerical solution is an iterative procedure, and $\tilde{\phi}_C$ converges toward the correct solution in the iterative procedure. As an interpolative function of $\tilde{\phi}_C$, $\tilde{\phi}_f$ should embody the variation of $\tilde{\phi}_C$ correctly to help the convergence of the solution effectively. Concretely, as a reasonable response to the change of $\tilde{\phi}_C$ for the interpolation, a small disturbance in $\tilde{\phi}_C$ should not generate an opposite directional disturbance in $\tilde{\phi}_f$. That is, $\tilde{\phi}_f$ should not decrease with increasing $\tilde{\phi}_C$. Corresponding to the SIR, this interpolation rule focuses on a reasonable dynamic response and is called dynamic interpolative reasonableness (DIR) here. We can clearly see that Eq. (15) in the CBC proposed by Gaskell and Lau [4] does not necessarily embody the dynamic interpolative reasonableness. Since $\phi_C$ is a normalized variable defined by Eq. (13), which is a function of $\phi_U$ at upstream point $U$, $\phi_C$ at central point $C$, and $\phi_D$ at downstream point $D$, Eq. (15) does not

provide the dynamic response of $\phi_f$ to the physical variable at a single grid point $U$, $C$, or $D$ concretely.

Now we see how the interpolation values $\phi_e$ at the cell face $e$ and $\phi_w$ at the cell face $w$, as shown in Figure 1, should respond correctly to the change of $\phi_P$ at a single central node $P$. The method of discrete perturbation analysis [17] is used to analyze the propagation characteristics of a localized disturbance. According to this method, when a disturbance is introduced at node $P$, no disturbance at the other two neighboring points $W$ and $E$ will be considered. Then the effect of this discrete perturbation at point $P$ on its neighboring grid points is examined. In order that a finite-difference solution be physically realistic, it is required that the sign of the resulting disturbances at nodes $W$ and $E$, propagated by the convection term and diffusion term indicated in Eq. (1), is the same as that of the disturbance imposed at node $P$ [18]. The sign preservation requirement sets a limit for the conditions under which a reasonable interpolation is applicable. Therefore, it is expected that the disturbances at cell faces $e$ and $w$ should have the same sign for the correct propagation of the disturbance imposed at node $P$ to the adjacent nodes $W$ and $E$. In other words, for a reasonable dynamic response, $\phi_e$ and $\phi_w$ should increase or decrease when $\phi_P$ increases or decreases, respectively. Thus we have

$$\begin{aligned} &\text{For } u \geq 0, \quad \frac{\partial \phi_e^+}{\partial \phi_P} = (0.75 + 2\alpha_e^+) \geq 0; \quad \frac{\partial \phi_w^+}{\partial \phi_P} = (0.375 - \alpha_w^+) \geq 0 \\ &\text{For } u < 0, \quad \frac{\partial \phi_e^-}{\partial \phi_P} = (0.375 - \alpha_e^-) \geq 0; \quad \frac{\partial \phi_w^-}{\partial \phi_P} = (0.75 + 2\alpha_w^-) \geq 0 \end{aligned} \tag{18}$$

In order not to violate the transportive property, the disturbance imposed on the central node $P$ should be propagated downstream by convection and diffusion and upstream only by diffusion. Therefore, the disturbance at an upstream cell face is expected to be less than or equal to that at a downstream cell face. Thus we have

$$\begin{aligned} &\text{For } u \geq 0, \quad \frac{\partial(\phi_w^+ - \phi_e^+)}{\partial \phi_P} = -0.375 - (\alpha_w^+ + 2\alpha_e^+) \leq 0 \\ &\text{For } u < 0, \quad \frac{\partial(\phi_e^- - \phi_w^-)}{\partial \phi_P} = -0.375 - (\alpha_e^- + 2\alpha_w^-) \leq 0 \end{aligned} \tag{19}$$

Combining Eqs. (18) and (19), finally we have

$$-0.125 \leq \alpha \leq 0.375 \tag{20}$$

## CONSTRAINTS FOR SCHEME WITH HIGH ORDER OF ACCURACY AND BOUNDEDNESS

From the aforementioned analyses, the following conditions should be satisfied in the NVD for the construction of a bounded, accurate scheme with interpolative reasonableness;

1. Convective boundedness criteria (CBC)
2. The scheme characteristics pass through point $(0.5, 0.75)$ for at least second-order accuracy
3. The maximum absolute value of variable parameter $\alpha$ in Eqs. (5) and (6) should be in the range of $[-0.125, 0.375]$ to satisfy the interpolative reasonableness

The above three conditions are named BAIR (Boundedness, Accuracy, and Interpolative Reasonableness) here, and the diagrammatic representation of BAIR is shown in Figure 4. In this plot, the hatched region and two parts of the first-order upwind line ($\hat{\phi}_c < 0$ and $\hat{\phi}_c > 1$) represent the BAIR. This means that if the characteristic line of a convection scheme is located within this hatched area for $\hat{\phi}_C \in [0, 1]$ and coincides with the first-order upwind line for $\hat{\phi}_C \notin [0, 1]$, the scheme possesses boundedness, at least of second-order accuracy and interpolative reasonableness. It is also noted that the BAIR region in the normalized variable diagram (NVD) contains three bottleneck points, $O(0, 0)$, $Q(0.25, 0.75)$, and $P(1, 1)$, which should be passed through for any high-resolution schemes.

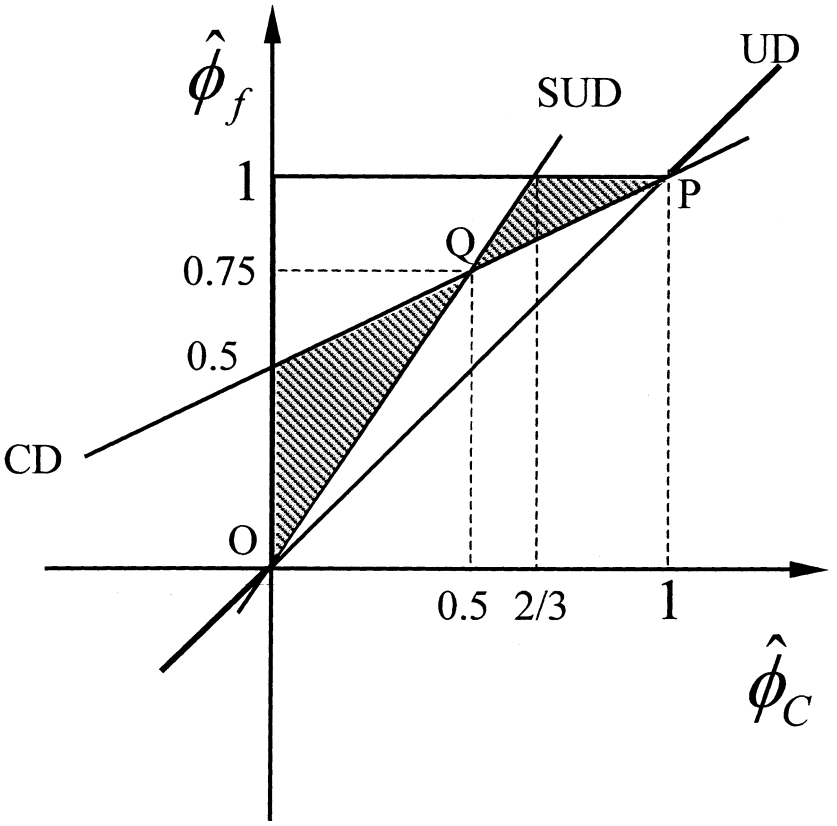


**Figure 4.** The region of BAIR.

## HOAB SCHEME

Following BAIR, one may choose several characteristic lines in the normalized variable diagram for high-resolution schemes. A number of high-resolution schemes have been proposed. Five often-used high-resolution schemes are listed in Table 2. From Table 2, it can be seen that in the NVD, any high-resolution scheme must be represented by a set of characteristic lines (either straight or curved), and all the lines fall into the BAIR region shown in Figure 5. When the scheme characteristic lines are near the first-order upwind line, the scheme tends to be highly diffusive, and the numerical diffusivity can be reduced by choosing the scheme characteristic line farther away from the first-order upwind line. For the five high-resolution schemes listed in Table 2, the recently proposed STOIC scheme with characteristic lines farthest away from the first-order upwind line was found to be the most accurate high-order scheme, and the MINMOD scheme with characteristic lines nearest the first-order upwind line was just the contrary. Therefore, it is expected that a more accurate bounded composite scheme could be found by further shifting the characteristics lines away from the first-order upwind line in the BAIR region shown in Figure 4. Based on this idea, a high-order-accurate and bounded scheme HOAB, is proposed in the present work as follows:

**Table 2.** High-resolution schemes

| High-resolution scheme | Expression | |
|---|---|---|
| MINMOD | $\hat{\phi}_f = 1.5\hat{\phi}_C$ | $0 < \hat{\phi}_C \leq 0.5$ |
| | $\hat{\phi}_f = 0.5\hat{\phi}_C + 0.5$ | $0.5 < \hat{\phi}_C < 1$ |
| | $\hat{\phi}_f = \hat{\phi}_C$ | elsewhere |
| CLAM | $\hat{\phi}_f = \hat{\phi}_C(2 - \hat{\phi}_C)$ | $0 < \hat{\phi}_C < 1$ |
| | $\hat{\phi}_f = \hat{\phi}_C$ | elsewhere |
| OSHER | $\hat{\phi}_f = 1.5\hat{\phi}_C$ | $0 < \hat{\phi}_C \leq 2/3$ |
| | $\hat{\phi}_f = 1$ | $2/3 < \hat{\phi}_C < 1$ |
| | $\hat{\phi}_f = \hat{\phi}_C$ | elsewhere |
| SMART | $\hat{\phi}_f = 3\hat{\phi}_C$ | $0 < \hat{\phi}_C \leq 1/6$ |
| | $\hat{\phi}_f = 0.75\hat{\phi}_C + 0.375$ | $1/6 < \hat{\phi}_C \leq 5/6$ |
| | $\hat{\phi}_f = 1$ | $5/6 < \hat{\phi}_C < 1$ |
| | $\hat{\phi}_f = \hat{\phi}_C$ | elsewhere |
| STOIC | $\hat{\phi}_f = 3\hat{\phi}_C$ | $0 < \hat{\phi}_C \leq 0.2$ |
| | $\hat{\phi}_f = 0.5\hat{\phi}_C + 0.5$ | $0.2 < \hat{\phi}_C \leq 0.5$ |
| | $\hat{\phi}_f = 0.75\hat{\phi}_C + 0.375$ | $0.5 < \hat{\phi}_C \leq 5/6$ |
| | $\hat{\phi}_f = 1$ | $5/6 < \hat{\phi}_C < 1$ |
| | $\hat{\phi}_f = \hat{\phi}_C$ | elsewhere |

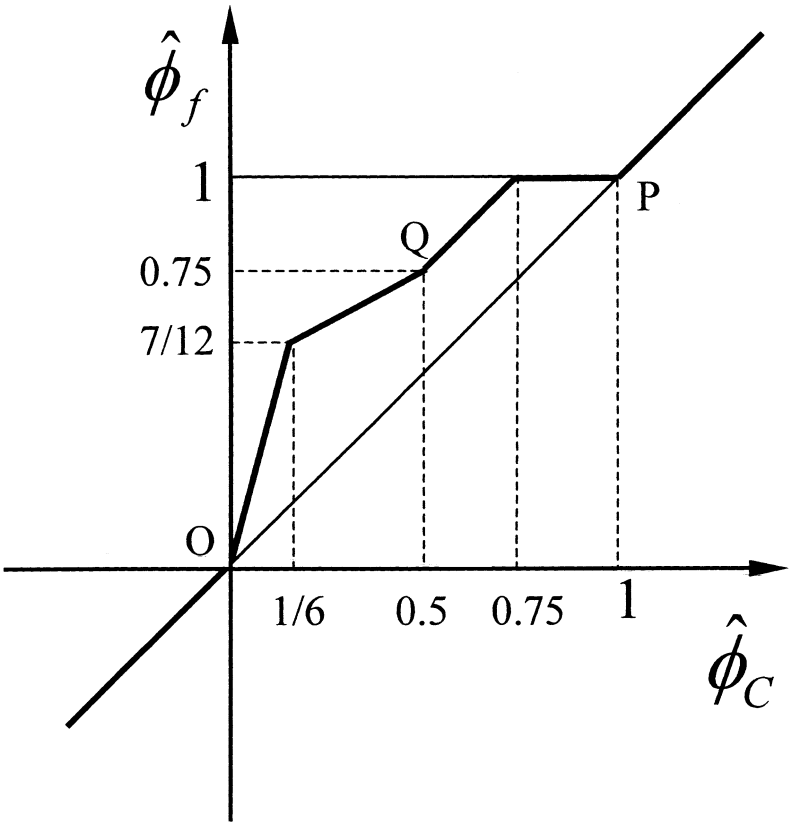


**Figure 5.** NVD plot for the HOAB scheme.

$$
\begin{aligned}
&\hat{\phi}_f = 3.5\hat{\phi}_C && 0 < \hat{\phi}_C \le 1/6 \\
&\hat{\phi}_f = 0.5\hat{\phi}_C + 0.5 && 1/6 < \hat{\phi}_C \le 0.5 \\
&\hat{\phi}_f = \hat{\phi}_C + 0.25 && 0.5 < \hat{\phi}_C \le 0.75 \\
&\hat{\phi}_f = 1 && 0.75 < \hat{\phi}_C < 1 \\
&\hat{\phi}_f = \hat{\phi}_C && \text{elsewhere}
\end{aligned} \tag{21}
$$

The scheme is represented in Figure 5. The above composite expressions can be rewritten as

$$
\begin{aligned}
&\phi_f = 3.5\phi_C - 2.5\phi_U && 0 < (\phi_C - \phi_U)/(\phi_D - \phi_U) \le 1/6 \\
&\phi_f = 0.5\phi_C + 0.5\phi_D && 1/6 < (\phi_C - \phi_U)/(\phi_D - \phi_U) \le 0.5 \\
&\phi_f = -0.25\phi_U + \phi_C + 0.25\phi_D && 0.5 < (\phi_C - \phi_U)/(\phi_D - \phi_U) \le 0.75 \\
&\phi_f = \phi_D && 0.75 < (\phi_C - \phi_U)/(\phi_D - \phi_U) < 1 \\
&\phi_f = \phi_C && \text{elsewhere}
\end{aligned} \tag{22}
$$

The differences between the HOAB scheme and the STOIC scheme are (1) in the region $0.5 < \hat{\phi}_C \leq 0.75$, Fromm's scheme [10] is used instead of the QUICK scheme; (2) the region of the central difference scheme becomes a little wider; and (3) the region of the downward scheme ($\hat{\phi}_f = 1$) also becomes a little wider. Although the scheme characteristic lines can be further shifted away from the first-order upwind line in the BAIR region, the NVD plot becomes very near the first-order downwind NVD plot (the line $\hat{\phi}_f = 1$) to make the scheme highly compressive. Our numerical tests show that this type of scheme often flattens the round profiles of physical variables and causes convergence problems. Thus the high-resolution (HR) scheme defined by Eq. (21) or (22) is preferred in the present study.

## TEST EXAMPLES

The HOAB scheme is applied to five test problems: (1) pure convection of a stepwise profile in an oblique uniform velocity field; (2) pure convection of a double-step profile in an oblique uniform velocity field; (3) pure convection of an elliptical profile in a given velocity field; (4) lid-driven cavity flows and (5) turbulent flow over a backward step. The first three problems are of pure convection, while the last two are of convection-diffusion for laminar and turbulent flow, respectively. Following are the performance comparisons of the HOAB scheme with the high-resolution schemes listed in Table 2. The aforementioned deferred-correction technique is used for the implementation of all the high-resolution schemes. The first-order upwind scheme is used whenever an upstream node lies outside the computational domain. A uniform grid with $21 \times 21$ meshes is used for the first four problems. The computational results are considered converged when the sum of the absolute residual error given by Eq. (23) becomes smaller than $10^{-6}$:

$$\mathrm{RES} = \frac{\sqrt{\sum \left| A_P \phi_P - \left( \sum_{\mathrm{NB}=E,W,N,S} A_{\mathrm{NB}} \phi_{\mathrm{NB}} + b \right) \right|^2}}{\sqrt{\sum (A_P \phi_P)^2}} \tag{23}$$

### Problem 1: Convection of a Stepwise Profile in an Oblique Uniform Velocity Field

Figure 6 shows the flow configuration of a well-known pure-convection test problem. This is the transportation of a scalar in a uniform oblique velocity filed. The magnitude of the velocity is unit. The flow angle is $35^\circ$. The boundary conditions for the calculated scalar $\phi$ are presented in Figure 6.

In order to compare the accuracy of different schemes quantitatively, we defined the following deviation:

$$\mathrm{ERR} = \sum_{\text{all grid points}} |\phi_{\text{exact}} - \phi_{\text{comput.}}| \tag{24}$$

A comparison of the scalar profiles at the mid-vertical plane ($x = 0.5$) predicted by the six high-resolution schemes is shown in Figure 7 along with the exact solution.

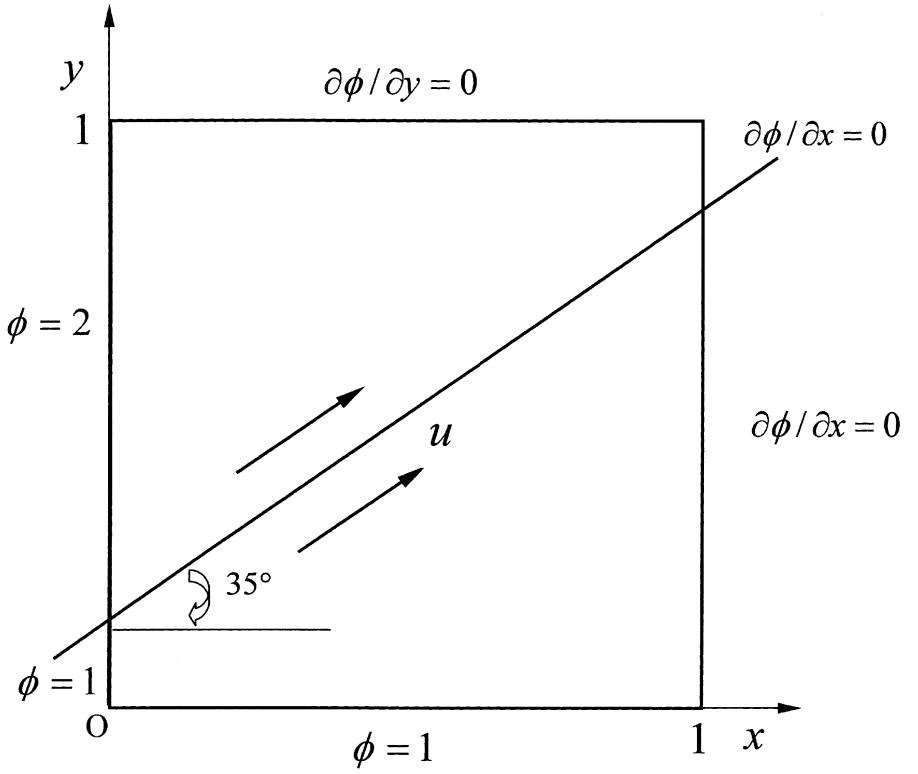


**Figure 6.** Pure convection of a step profile in a uniform velocity.

The MINMOD results in a relatively very diffusive $\phi$ profile due solely to the influence of artificial (numerical) diffusion, while the new proposed scheme HOAB can capture steep change of $\phi$ profile most accurately. Table 3 further gives the error comparisons to assess the different schemes more accurately. Corresponding to the prediction in Figure 7, it is seen that the error of HOAB scheme is the least and less than half of the maximum error of MINMOD. The error decreases in the order MINMOD, CLAM, OSHER, SMART, STOIC, and HOAB.

### Problem 2: Pure Convection of a Double-Step Profile

Figure 8 presents the second test problem, consisting of pure convection of a transverse double-step (up-step and down-step) profile imposed at the inflow boundaries of a square computational domain. This test problem is very similar to the first one. The major difference lies in that there exists a down step in the profile. The flow angle is 45°. Table 4 provides the error comparison [error defined by Eq. (24)] for the six HR schemes. Figure 9 compares the predicted scalar profiles at the mid-vertical plane ($x = 0.5$) with the exact solution. Similar to the test results obtained in problem 1, the MINMOD cannot predict the sharp profile very well due to its relatively high numerical diffusion, while the sharp gradient in $\phi$ is again best preserved by using the HOAB scheme. The error decreases in the order MINMOD,

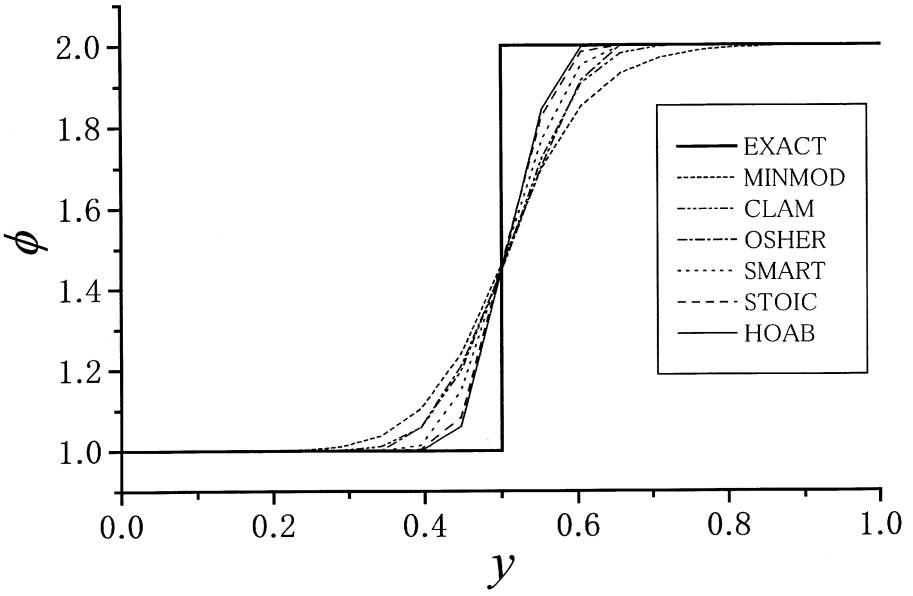


**Figure 7.** Scalar profiles at the mid-vertical plane ($x = 0.5$) for problem 1.

CLAM, OSHER, SMART, STOIC, and HOAB. The error of the MINMOD is more than twice that of the HOAB and STOIC schemes.

### Problem 3: Convection of an Elliptical Profile

Both the former two test problems show that MINMOD is the most diffusive, and the numerical diffusion could be reduced by the HR schemes with characteristics lines farther away from the first-order upwind line in the BAIR region shown in Figure 4, and the most accurate result is obtained by the new proposed HOAB scheme, the characteristics line of which is the farthest away from the first-order upwind line. However, by doing this, the NVD plot becomes near to the first-order downwind NVD plot (the line $\hat{\phi}_f = 1$), making the scheme highly compressive, which may flatten the round distribution of physical variables due to substantial false compression, as pointed out by Darwish [8]. The step distribution in the former two tests cannot test this effect. Thus, in test problem 3, pure convection of an elliptical profile in a given velocity field is calculated. Figure 10 shows the problem schematically. Figure 11 compares the calculated scalar profiles at the outlet vertical plane ($x = 1$). Although a slight flattening of the profile can be observed in the HOAB and STOIC schemes, the two schemes give better predictions than the other four schemes and the HOAB gives the closest resemblance of its $\phi$ profile to the exact solution

**Table 3.** Error comparison for problem 1

| Scheme | HOAB | STOIC | SMART | OSHER | CLAM | MINMOD |
|---|---|---|---|---|---|---|
| ERR | 11.35 | 12.47 | 16.02 | 19.88 | 19.86 | 25.02 |

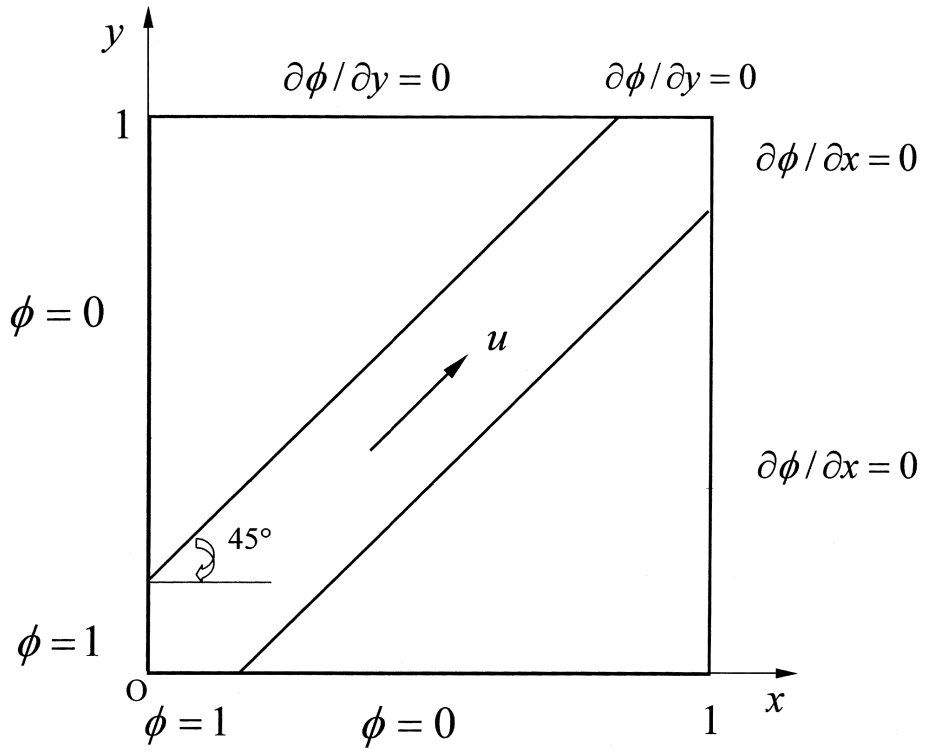


**Figure 8.** Pure convection of a double-step profile in a uniform velocity.

profile. Therefore, the new proposed HOAB scheme may be a reasonable compromise between diffusive and compressive performance.

### Problem 4: Lid-Driven Flow in a Square Cavity

The former three test problems with pure convection are for examining the relative performance of the numerical approximations of the HOAB scheme. The problem with both convection and diffusion should be tested, since it is general in CFD/NHT. Despite its simple geometry and boundary conditions, driven flow in a square cavity is widely used as a test case because of its complex flow pattern. The problem is depicted schematically in Figure 12. Calculations are carried out for Reynolds numbers of 100, 1,000, and 5,000. The Reynolds number is defined as $\mathrm{Re} = \rho U_0 L/\mu$, where $L$ is the length of the cavity and $U_0$ is the velocity at the top moving wall. Figure 13 shows the comparison of the vertical velocity profiles along the horizontal cavity centerline. The benchmark solutions of Ghia et al. [19] are also

**Table 4.** Error comparison for problem 2

| Scheme | HOAB | STOIC | SMART | OSHER | CLAM | MINMOD |
|---|---|---|---|---|---|---|
| ERR | 21.88 | 24.69 | 34.64 | 41.83 | 43.68 | 54.03 |

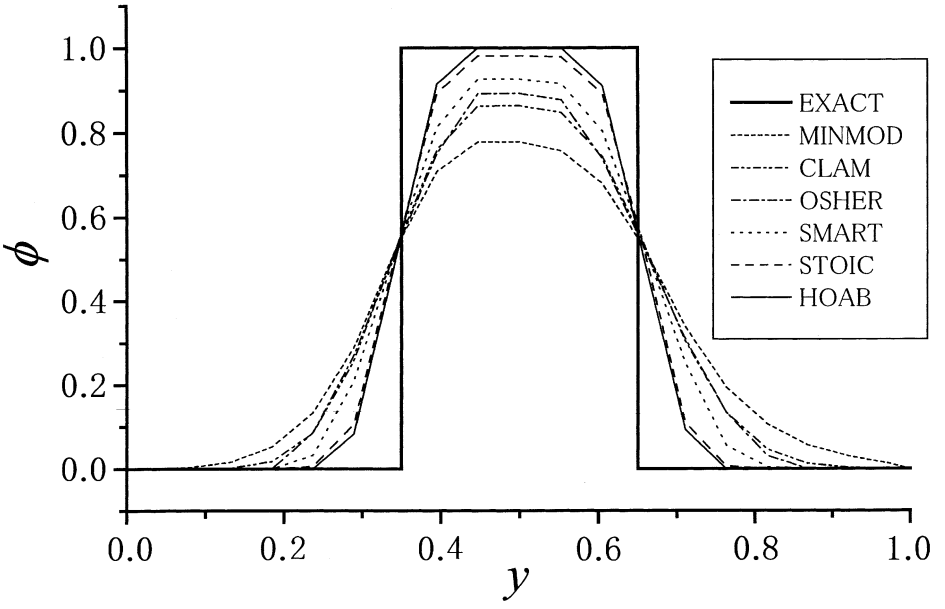


**Figure 9.** Scalar profiles at the mid-vertical plane ($x = 0.5$) for problem 2.

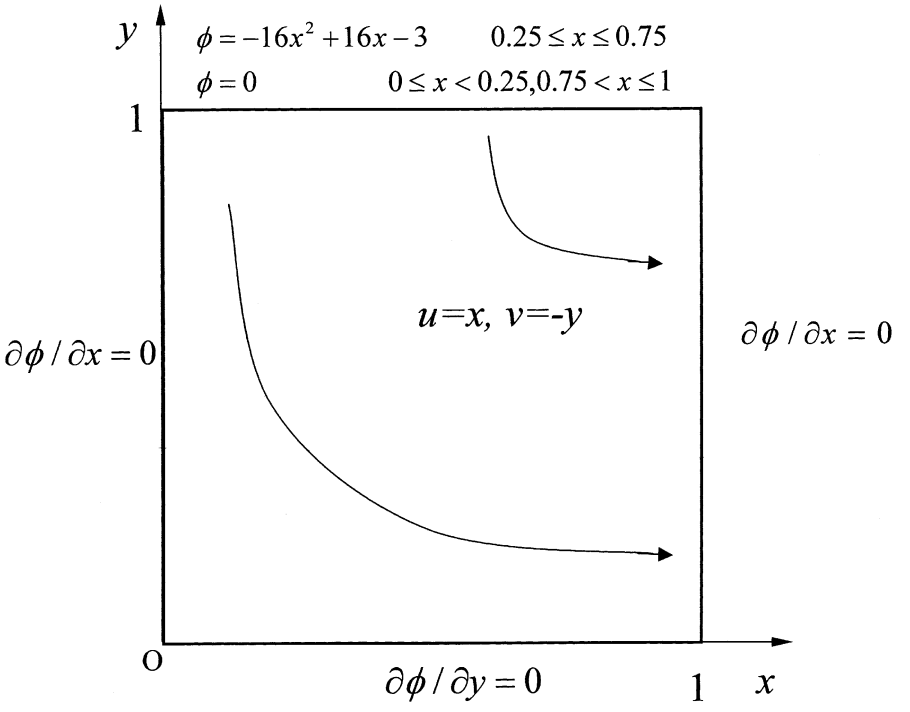


**Figure 10.** Pure convection of an elliptical profile.

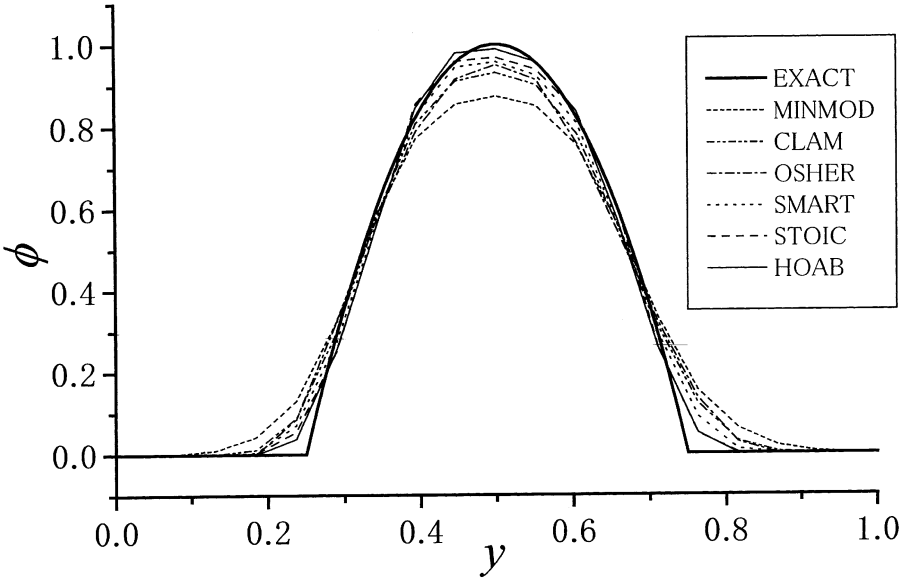


**Figure 11.** Scalar profiles at the outlet vertical plane ($x = 1.0$) for problem 3.

shown. This example shows for the small Reynolds number of 100, all the schemes have similar accuracy, with the HOAB scheme slightly more accurate. For the moderate Reynolds number of 1,000 and the high Reynolds number of 5,000, the HOAB scheme has superior accuracy to the other five HR schemes. As is expected, the accuracy of the MINMOD scheme is the lowest. Since lid-driven square cavity flow has strong elliptical character, the test results also show that the HOAB scheme is very good for elliptical problems.

In all the above calculations, a coarse $21 \times 21$ mesh is used. We also checked the effect of the grid numbers. Using a $41 \times 41$ mesh, the same conclusion is obtained. For brevity, we do not present those results here.

### Problem 5: Turbulent Flow over a Backward-Facing Step

The two-dimensional flow over a backward-facing step is a typical flow field that contains the basic separation-reattachment characteristics. Despite the simple geometry, the flow behind the backward-facing step is quite complex and contains many basic features of scientific and engineering interest. Therefore, it has been widely selected for the evaluation of numerical methods and turbulence models. To evaluate the performance of the new proposed scheme HOAB, a turbulent case is used for comparison. A schematic of the problem is shown in Figure 14. The expansion ratio is 1.5 and the step height $H$ is 3.5 cm. Inlet bulk velocity $U_{\text{in}} = 75$ m/s. The inlet location is at $4H$ upstream of the step corner and the exit is at $16H$ of the step. Numerical computations are performed with standard $k-\varepsilon$ turbulence model on the $40 \times 30$ uniform grids.

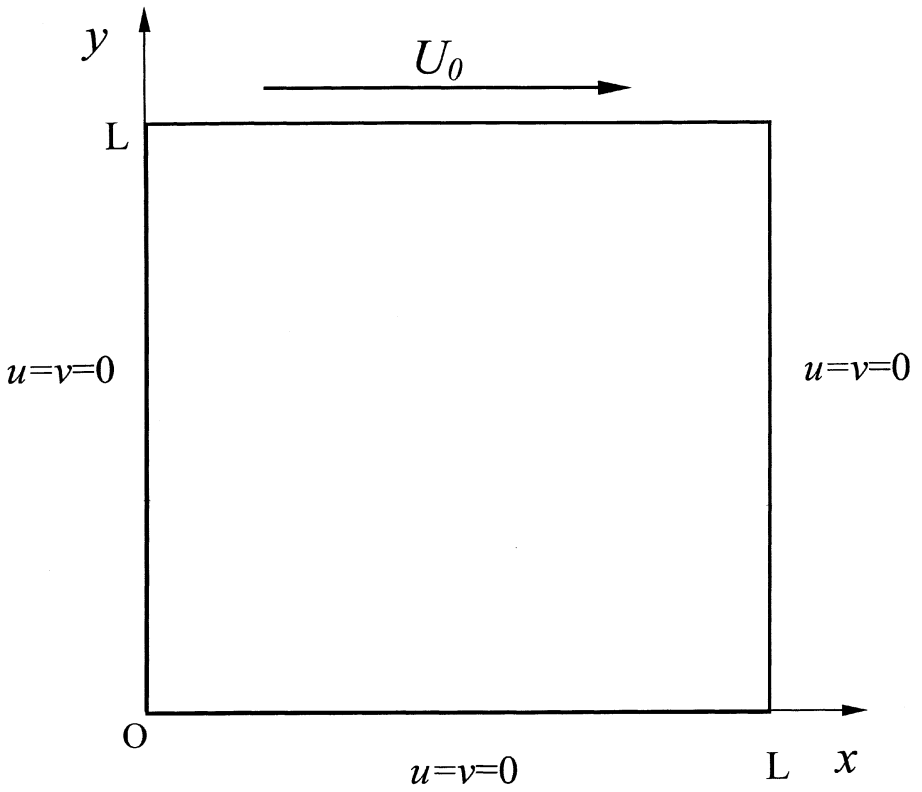


**Figure 12.** Lid-driven flow in a square cavity.

The reattachment length is the most important parameter in backward-facing step flow, and comparisons of the predictive dimensionless reattachment length, $x_R/H$, are listed in Table 5. The prediction of Chao and Liu [20] with a hybrid scheme and prediction with a first upwind scheme are also shown in Table 5. When compared with the experiment data, $x_R/H = 7.33$, the result by the new proposed HOAB scheme is the most accurate. It is noticed that all the schemes underpredict the reattachment lengths by a large amount. The origin of these discrepancies may come from the uncertainty of the experimental measurement, the inadequacy of the $k-\varepsilon$ model in the recirculation zone, and insufficient grid number. Eaton [21] found that the reattachment length is underpredicted by all $k-\varepsilon$ models by about 20% ($x_R/H = 5.86$), due to the lack of sensitivity of the $k-\varepsilon$ model to the streamline curvature.

Figure 15 shows the comparison of dimensionless $x$-directional velocity distribution at various locations $x/H = 0.73$, 5.13, 7.33, and 10.23. Due to the limited capability of the standard $k-\varepsilon$ model, all the predicted velocity distributions in the recirculation zone lag behind the experimental data. Despite this, all the high-order schemes predict the velocity distribution much better than did the first upwind scheme. Corresponding to the prediction of reattachment length, the predicted result

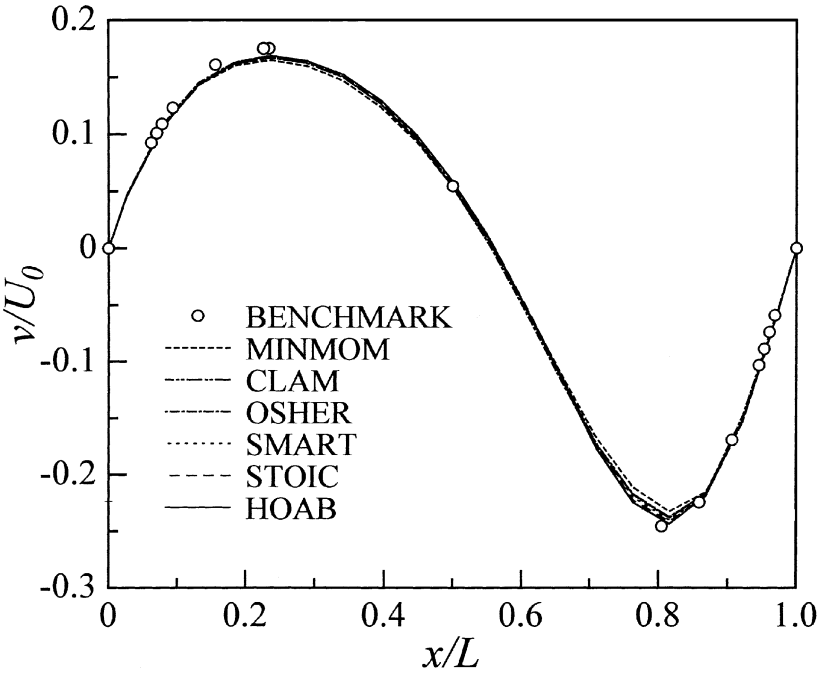


(a) Re=100

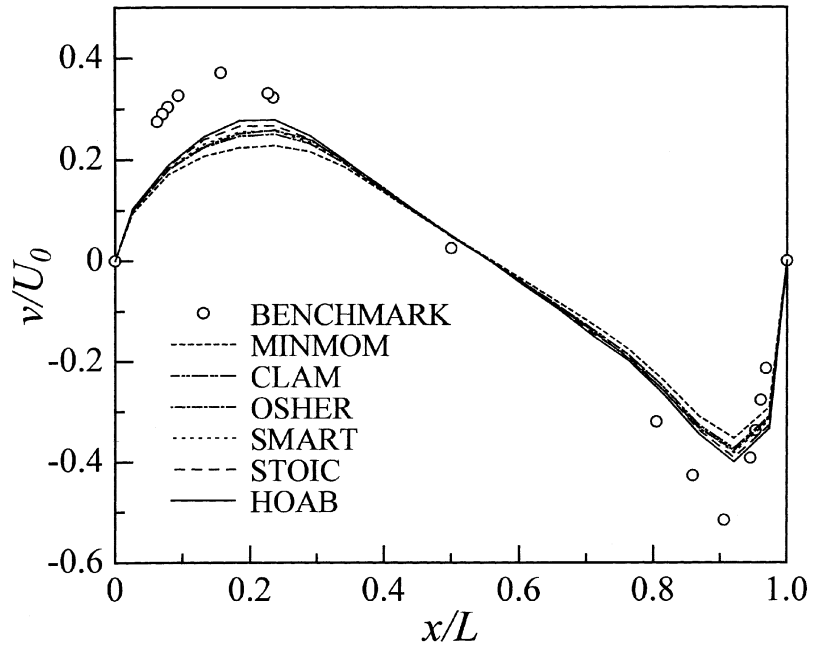


(b) Re=1000

**Figure 13*a–b*.** Vertical velocity profile along the cavity horizontal centerline ($y/L = 0.5$) for problem 4: (*a*) Re = 100; (*b*) Re = 1,000.

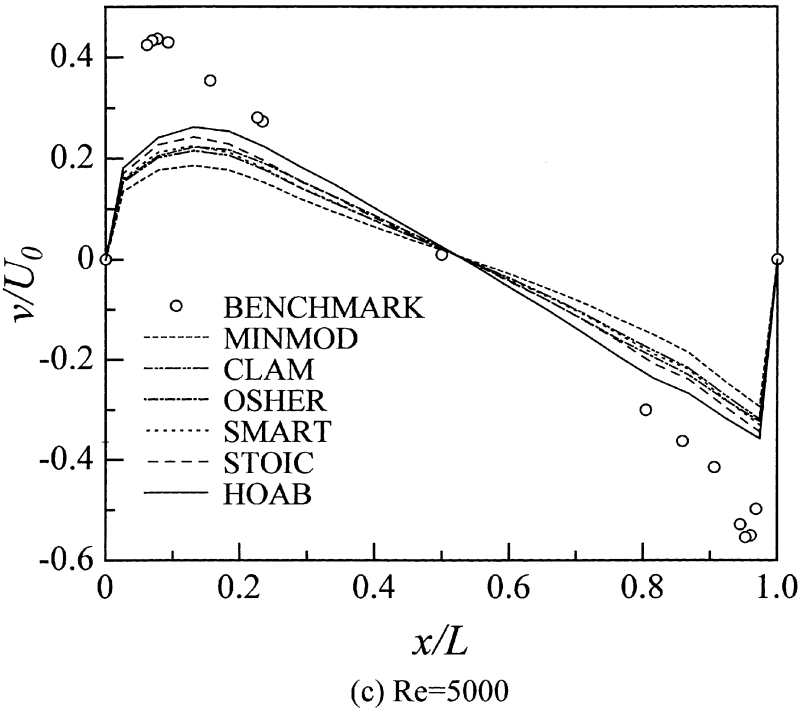


**Figure 13*c*.** Vertical velocity profile along the cavity horizontal centerline ($y/L = 0.5$) for problem 4: (*c*) $\mathrm{Re} = 5{,}000$.

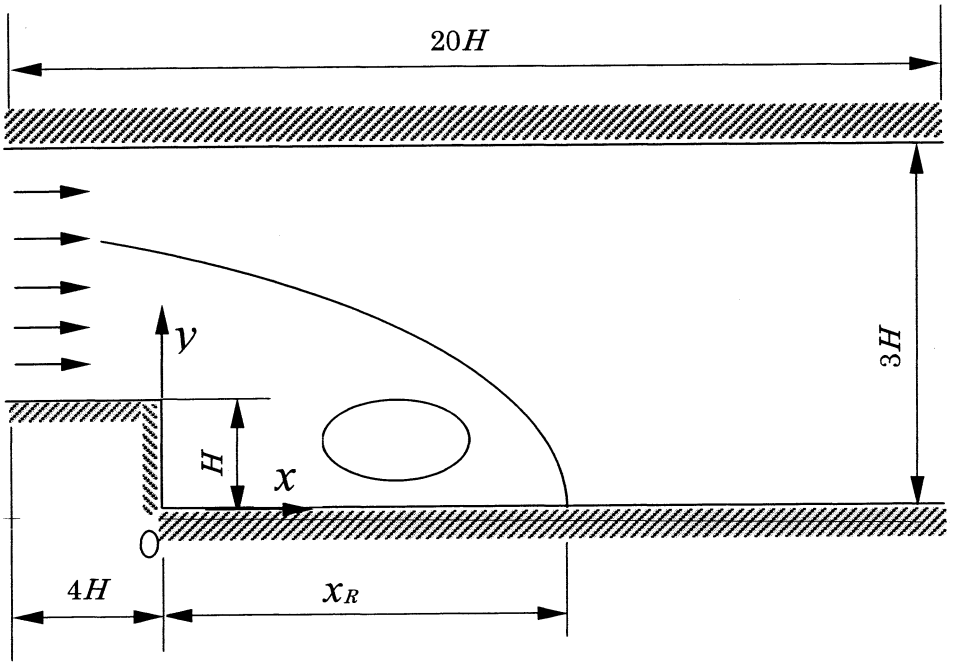


**Figure 14.** Schematic of backward-facing step.

**Table 5.** Comparison of reattachment length on the $40 \times 30$ grid

| Scheme | HOAB | STOIC | SMART | OSHER | CLAM | MINMOD | Hybrid | FUD |
|---|---|---|---|---|---|---|---|---|
| $x_R/H$ | 5.405 | 5.396 | 5.377 | 5.369 | 5.357 | 5.304 | 4.820 | 4.607 |

accuracy increases in the order MINMOD, CLAM, OSHER, SMART, STOIC, and HOAB. Since the differences of the predicted results for all the high-order schemes are small, for clarity, only the results of HOAB, MINMOD, and the first upwind schemes are given in Figure 15. The other results lie in between those of HOAB and MINMOD.

This test shows that the new proposed HOAB scheme is also the most accurate for the computation of complex turbulent flow among the six high-order schemes in this study.

## CONCLUSIONS

From the viewpoint of iterative procedure, a constraint for designing a discretization scheme of convective terms is proposed: the interfacial variable should have a positive response to the disturbance of variable at grid points and the transportive property should be kept (called dynamic interpolative reasonableness, DIR). Combining this constraint with the CBC and the requirement of going through the point $Q$, a new set of conditions for designing a bounded and accurate scheme with interpolative reasonableness (BAIR) is proposed which can guarantee the scheme to be bounded and at least of second-order accuracy.

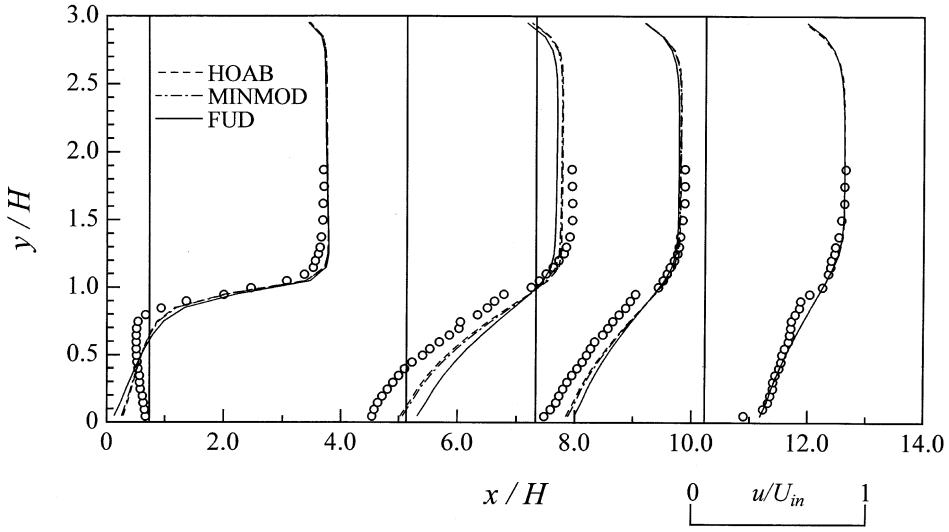


**Figure 15.** Comparison of velocity distribution for problem 5.

A high-resolution convective scheme based on the conditions of BAIR, HOAB, is formulated for the calculation of incompressible steady-state transport problems. The accuracy of the scheme is verified for five test problems. Numerical experiments show that the proposed scheme yields more accurate results than any other high-resolution scheme compared (MINMOD, CLAM, OSHER, SMART, and STOIC). In addition, no nonphysical oscillation was predicted by the scheme.

## REFERENCES


1. C. J. Freitas, Editorial, *ASME J. Fluids Eng.*, vol. 115, pp. 339–340, 1993.
2. B. P. Leonard and J. E. Drummond, Why You Should Not Use Hybrid, Power-Law or Related Exponential Schemes for Convective Modeling—There Are Much Better Alternatives, *Int. J. Numer. Meth. Fluids*, vol. 20, pp. 421–442, 1995.
3. J. H. Ferziger and M. Peric, *Computational Methods for Fluid Dynamics*, p. 84, Springer, Berlin, 1996.
4. P. H. Gaskell and A. K. C. Lau, Curvature-Compensated Convective Transport: SMART, a New Boundedness-Perserving Transport Algorithm, *Int. J. Numer. Meth. Fluids*, vol. 8, pp. 617–641, 1988.
5. J. Zhu and W. Rodi, A Low-Dispersion and Bounded Convection Scheme, *Comput. Meth. Appl. Mech. Eng.*, vol. 92, pp. 87–96, 1991.
6. B. Van Leer, Towards the Ultimate Conservative Difference Scheme II. Monotonicity and Conservation Combined in a Second Order Scheme, *J. Comput. Phys.*, vol. 14, pp. 361–370, 1974.
7. S. R. Chakravarthy and S. Osher, High-Resolution of the OSHER Upwind Scheme for the Euler Equations, pp. 83–94, *AIAA Paper* 83-1943, 1983.
8. M. S. Darwish, A New High-Resolution Scheme Based on the Normalized Variable Formulation, *Numer. Heat Transfer B*, vol. 24, pp. 353–373, 1993.
9. B. Song, G. R. Liu, K. Y. Lam, and R. S. Amano, On a Higher-Order Bounded Discretization Scheme, *Int. J. Numer. Meth. Fluids*, vol. 32, pp. 881–897, 2000.
10. J. E. Fromm, A Method for Reducing Dispersion in Convective Difference Schemes, *J. Comput. Phys.*, vol. 3, pp. 176–189, 1968.
11. B. P. Leonard, A Stable and Accurate Convective Modeling Procedure Based on Quadratic Upstream Interpolation, *Comput. Meth. Appl. Mech. Eng.*, vol. 19, pp. 59–98, 1979.
12. P. K. Khosla and S. G. Rubin, A Diagonally Dominant Second Order Accurate Implicit Scheme, *Comput. Fluids*, vol. 2, pp. 207–209, 1974.
13. B. P. Leonard, Locally Modified QUICK for Highly Convective 2-D and 3-D Flows, in K. Morgan (Ed.), *Numerical Methods in Laminar and Turbulent Flow*, Pineridge Press, Swansea, 1987.
14. B. Yu, W. Q. Tao, D. S. Zhang, and Q. W. Wang, Discussion on Numerical Stability and Boundedness of Convective Discretized Scheme, *Numer. Heat Transfer B*, vol. 40, pp. 343–365, 2001.
15. B. P. Leonard, The ULTIMATE Conservative Difference Scheme Applied to Unsteady One Dimension Advection, *Comput. Meth. Appl. Mech. Eng.*, vol. 88, pp. 17–74, 1991.
16. W. Q. Tao, *Recent Advances in Computational Heat Transfer*, Science Press, Beijing, 2000.
17. W. Q. Tao, *Numerical Heat Transfer*, 2d ed., Xi'an Jiaotong Press, Xi'an, China, 2001.
18. W. Q. Tao and E. M. Sparrow, The Transportive Property and Convective Numerical Stability of the Steady-State Convection-Diffusion Finite-Difference Equation, *Numer. Heat Transfer B*, vol. 11, pp. 491–497, 1987.

19. U. Ghia, K. N. Ghia, and C. T. Shin, High-Re Solutions for Incompressible Flow Using the Navier Stokes Equations and a Multigrid Method, *J. Comput. Phys.*, vol. 48, pp. 387–411, 1982.
20. Y. C. Chao and S. S. Liu, Streamline Adaptive Grid Method for Complex Flow Computation, *Numer. Heat Transfer B*, vol. 20, pp. 145–168, 1991.
21. J. K. Eaton, Incompressible Separated Flows-Internal Flows-Backward-Facing Step, *1980–81 AFOSR-HTTM-Stanford Conf. on Complex Turbulent Flows*, Stanford University, Stanford, CA, vol. 2, pp. 886–904, 1981.